COMMUNICATIONS IN SCIENCE AND TECHNOLOGY
Homepage: cst.kipmi.or.id

Simulation and optimization of fatty acid extraction parameters from *Nannochloropsis sp.* using supercritical carbon dioxide

Ivander Jonathan Kim, Aris Romadhon Subkhan, Rakha Putra Prasetya, Yuswan Muharam*

Department of Chemical Engineering, Universitas Indonesia, Depok 16424, Indonesia

Article history:
Received: 1 April 2024 / Received in revised form: 23 June 2024 / Accepted: 25 June 2024

Abstract

Microalgae, which are rich in fatty acids, have potential applications in various sectors such as bioenergy, health, food, and biomaterials. The Supercritical Fluid Extraction (SFE) method is commonly used to extract microalgae. This research estimated the process parameters of desorption rate constant (k_d) and binary diffusion coefficient (D_{AB}) for SFE fatty acid from *Nannochloropsis sp*. using a mathematical model called as hot sphere diffusion. Desorption models were used to model the release of fatty acids into the solvent (supercritical carbon dioxide). The parameter estimation process was conducted at temperatures of 313 and 333 K and pressures of 12.5, 20, and 30 MPa. The value of k_d increased with increasing pressure and temperature and D_{AB} values were obtained at varying pressures and temperatures.

Keywords: Fatty acid; supercritical fluid extraction; supercritical carbon dioxide; hot sphere diffusion; process parameter estimation

1. Introduction

Microalgae are microorganisms with considerable potential as a source of production for various sectors, including biotechnology, biodiesel, supplements, nutritional foods, supplements, and cosmetics. They have high value algal metabolites (HVAMs) that are able to reduce CO_2 levels for human activity [1]. Microalgae represent a third-generation renewable energy source that does not compete with human and industrial primary needs. In terms of energy conversion, they can produce 15 to 300 times more biofuel than first- and second-generation renewable energy sources with the same land area [2]. Microalgae is known to have fast- and cost-effective photosynthetic growth [3]. The potential of microalgae can be observed in the high fatty acid content, which can reach 31–68% of its dry weight [4]. *Nannochloropsis sp.* is one of the marine microalgae that is easily cultivated with a short harvest period [5]. It can be extracted through methods such as microwave-assisted extraction, enzymatic-assisted extraction, ultrasound-assisted extraction, pressurized liquid extraction, and supercritical fluid extraction [6]. The growth process of *Nannochloropsis sp.* by fixing free CO_2 can assist in the minimization of global warming. Microalgae exhibit a CO_2 binding efficiency that is approximately ten times greater than that of ordinary plants [7].

The fatty acid content of *Nannochloropsis sp.* can be obtained by extraction. The conventional method of fatty acid extraction from microalgae is by using organic solvents or Soxhlet extraction. However, there is a growing trend towards the use of supercritical fluid extraction (SFE), which offers several advantages over traditional methods. Supercritical carbon dioxide is the most used fluid as a solvent due to its non-toxic, odorless and residue-free properties. A considerable number of studies have employed supercritical fluids to extract fatty acids and bioactive compounds from microalgae. For instance, fatty acid extraction from *Nannochloropsis sp.* [8], carotenoid extraction from *Dunaliella salina* [9], fucosanthin extraction from *Sargassum muticum* [10], fat extraction from *Scenedesmus obliquus* [11], nonpolar pigments and fats from *Nannochloropsis gaditana* [12], oil extraction from *Asterias rubens* by Getachew et al. [13], and extraction from *L. rivularis* stalks by Uguiche et al. [14] have been successfully modeled, and fat extraction from *Dunaliella salina* [9] have been successfully achieved. Indeed, numerous researchers have employed simulation and modelling techniques to investigate SFE, including the extraction of carotenoids from *Nannochloropsis gaditana, Synechococcus,* and *Dunaliella salina* [15]. Another method that has been used for the extraction of bioactive compounds is ultrasound-assisted enzymatic extraction of flavonoids from *Strobilanthes crispus* by Arbianti et al. [16].

The SFE process can be expressed using mathematical models. Mathematical modelling of SFE is one of the tools that can help optimization and scale-up from laboratory scale to

* Corresponding author.
Email: muharam@che.ui.ac.id
https://doi.org/10.21924/cst.9.1.2024.1420

industrial scale. With mathematical modelling, the effect or impact of process parameters on yield and extraction rate can be determined. Mathematical models for SFE can be divided into three main categories: empirical models, models based on mass and energy transfer analogies, and models based on the integration of mass balance differential equations. These mathematical models can be used to estimate appropriate process parameters based on experimental operating conditions. The independent variables, operation conditions, and models describing the progress of the extraction over time makes the simulation process possible. The particles were depicted as spheres so the mass transfer phenomena in the biomass can be described as shrinking core models, broken and intact cell models, linear driving force models, or a combination of all [17].

The use of mathematical models for carotenoid extraction from *Nannochloropsis gaditana* was conducted by Macias-Sanchez, et al. [15] using the mass transfer model of the penetration method. This modelling was employed to estimate the process parameters. The process parameters obtained were diffusivity of (1.24 - 14) × 10^{-18} m^2/s at pressures of 100-500 bar and temperatures of 40-60℃. However, the deviation of the application of this model to the experiments conducted was 25%. Another mathematical model used by Mouahid et al. [18] is Sovova's mathematical model for the extraction modelling for N. salina and N. maritima with a mass transfer coefficient pf 7.695 × 10^{-5}/s and 8.833 × 10^{-5}/s at 300 bar and 333K, respectively.

There is still a scarcity of mathematical modelling of SFE from microalgae. The modelling of carotenoid extraction from *Nannochloropsis gaditana* by Macias-Sanchez, et al. [15] still exhibits a considerable deviation value. Here, the value obtained for the binary diffusivity (10^{-19} m^2/s) was still relatively low when compared to SFE modelling of other biomass, such as grains (10^{-10} to 10^{-14} m^2/s) [19]. The modelling of oil extraction from *Citrus auranticum* L. by Kusuma, et al. [20] is the second-order model. The value obtained for the extraction rate constant was 1.4075 L g^{-1} m^{-1}. The mass transfer model of *Scenedesmus sp.* Lipids extraction by Taher, et al. [21] utilized the broken and intact cells (BIC) model for predicting extraction curves. The values obtained for the mass transfer coefficients in the fluid and solid phases were in the ranges of 6.7 - 30.9 × 10^{-6} m/s and 2.08 - 13.2 × 10^{-10} m/s, respectively. The modelling for extracting lipid from *Chlorella vulgaris* NIES 227 microalgae by Wetterwald, et al. [22] with the BIC model. The results shows that Soxhlet extraction with hexane had higher lipid yields at 31.20 wt% extract/dry biomass. Considering these limitations, this study aimed to perform the mathematical modelling of fatty acid extraction from *Nannochloropsis sp.* to identify optimal process parameters. The experiment to be modelled was derived from the fatty acid extraction that has been carried out by Nobre, et al. [8]. The objective of this modelling is to identify the process parameters such as desorption rate coefficient and solute diffusivity in the solvent of SFE.

2. Materials and Methods

The study employed a 3D packed bed reactor extractor model from the COMSOL Multiphysics chemical reaction engineering module, based on the research conducted by Nobre et al. [6]. The template was adjusted to account for extractor and particle dimensions, bed porosity, solvent feed flow rate, solvent density, and viscosity. The assumptions used included 1D axisymmetric extractor model, perfectly spherical solid matrix, the transfer of fatty acids in the solid based on the desorption principle, isothermal extraction process, analogous solid matrix to a hot ball that uniformly cools the environment, and the lipid composition of the experimental results from Nobre et al. [8], which consisted only of fatty acids without glycerol.

2.1. Extractor mass scale balance

Phenomena occurred at the extractor scale include flow transfer by convection and molecular diffusion. Convection flow transfer occurs when fluid flows in the bulk phase with a speed of u. Meanwhile, diffusion occurs due to the fluid concentration gradient formed in the film layer (gas-solid interface). In this model, convection and diffusion in the radial direction are ignored. The mass flow rate at the inlet and outlet is based solely on convection and diffusion in the axial direction. The overall mass balance equation is presented by Equation (1).

$$\varepsilon \frac{\partial C_b}{\partial t} = \varepsilon D_L \frac{\partial^2 C_b}{\partial z^2} - u_{sup} \frac{\partial C_b}{\partial z} + (1-\varepsilon) k_f a_p \left(C_p - C_b\right) \quad (1)$$

2.2. Mass balance in film layer

The correlation between the mass transfer in the extractor scale phases (bulk) and the mass flux at the particle surface (pores) models the mass balance in the film layer. It is assumed that there is no external resistance in this layer, so the first derivative of the concentration gradient in the pore is given entirely to the bulk. Equation (2) represents this phenomenon.

$$k_f a_p \left(C_p - C_b\right) = a_p D_e \frac{\partial C_p}{\partial r} \quad (2)$$

2.3. Particle scale mass balance

In particle systems, the fluid diffuses into the pores of the particles, providing a site for the reaction to occur. The fatty acid solute is then carried out by the fluid. This particle-scale model considers only the mass balance equation. As the particles are in the solid phase, the transfer phenomenon that occurs is limited to radial diffusion through the particle pores. Particle-scale mass balance is divided into two, namely in the pore and in the solid. The mass balance in the pore follows Equation (3) and the mass balance in the solid follows Equation (4).

$$\varepsilon_p \frac{\partial C_p}{\partial t} + \left(1-\varepsilon_p\right) \frac{\partial q}{\partial t} = \frac{\varepsilon_p D_e}{r^2} \frac{\partial}{\partial t} \left(r^2 \frac{\partial C_p}{\partial r}\right) \quad (3)$$

$$\left(1-\varepsilon_p\right) \frac{\partial q}{\partial t} = -k_d q \quad (4)$$

2.4. Mass transfer modelling parameters

The Sherwood number empirical correlation by Frossling

was used to estimate the mass transfer coefficient in a stationary bed extractor with supercritical CO_2.

$$Sh = 2 + 0{,}55^{0{,}33} Re^{0{,}5} \quad (5)$$

where

$$Sh = \frac{2 r_p k_f}{D_A B} \quad (6)$$

and

$$Sc = \frac{\mu}{\rho D_{AB}} \quad (7)$$

The Peclet number correlation was used to approximate the axial dispersion coefficient at supercritical conditions.

$$Pe = 0{,}187 Re^{0{,}265} Sc^{-0{,}919} \quad (8)$$

where

$$Pe = \frac{2 r_p u_{sup}}{D_L} \quad (9)$$

The effective diffusion coefficient of the particles was determined by following Millington and Quirk's statement.

$$D_e = \varepsilon^{1{,}333} D_{AB} \quad (10)$$

2.5. Model verification and simulation

Once the mass balance of the model has been obtained, the next step was to verify the model. This involves determining whether the model could be run by COMSOL. If it could be run, the research continued to the simulation stage. However, if there were still errors, it was necessary to check the parameter input in the model. Some of the errors that can cause a run to fail include punctuation errors, unit factors, duration of the simulation run, convergence tolerance, or variables that have not been entered.

A simulation was carried out when the model verification results were valid. The model was stated valid if the results of running the program do not bring up error messages. At this stage, a simulation was carried out with operating conditions according to Nobre, et al.'s research [8] with an aim to estimate the process parameters, specifically the desorption rate constant (k_d) and solute diffusivity coefficient in solvent (D_{AB}). The outcome of this simulation was an instantaneous concentration curve at the extractor output. This curve would be compared with the experimental results of Nobre, et al. [8] in the form of a yield accumulation curve.

3. Results and Discussion

3.1. Parameter input and condition operation

The process of extracting fatty acids from solid particles/matrix into bed gaps occurs under constant temperature conditions, ensuring no changes in temperature or energy. This is similar to a hot ball cooling the environment uniformly. The process moves fatty acids from the spherical core to the surface and then out into the bed gap. The simulation assumes that the lipid composition consists solely of fatty acids without glycerol, as there is no data explaining the glycerol content in the experimental results. Table 1 presents the assumptions used to describe the composition of the extract and Table 2 presents the operating conditions of the Nobre et al. [8] experiments and details the parameter values used in their modelling, which were entered into COMSOL to ensure that the extractor geometry and modelled particles were considered experimental data.

Table 1. Composition of the fatty acid extracts [6]

Compound	Name	Percentage (%)
C16:0	Palmitic Acid	35.29
C16:1	Palmitoleic Acid	36.92
C18:1	Oleic Acid	18.41
C14:0	Miristic Acid	4.37
C20:5	Eicosapentonic Acid	2.93
C20:4	Arachidonic	1.84

Table 2. SFE Operation Conditions and Parameters [6]

Name	Value
Feed Temperature	313 and 333 K
Feed Pressure	12.5, 20, and 30 MPa
Feed Flow Rate	0.35 gr/minute
Extractor Length	102 m
Extractor Radius	3.95 nm
Particle Radius	1.5×10^{-5} m
Particle Porosity	0.15
Fixed bed porosity (ε)	0.40019
Area of extractor's cross section (A_c)	4.0917×10^{-5} m^2
Superficial velocity (u_{sup})	1.6263×10^{-4} m/s

3.2. Effect of pressure and temperature on parameter k

Desorption is the release of adsorbate/solute (in this case, fatty acids) past the surface of the solid matrix. The driving force of the desorption process is the concentration gradient between the fluid in the pore and the solid. This concentration gradient is determined by the partial pressure of the fluid in the pore and the vapor pressure in the solid. Increasing the pressure will increase the fluid concentration in the pore as the solvation strength rises. Assuming that the concentration in the solid is constant due to its high value, an increase in pressure will result in a reduction in the concentration gradient between the fluid in the pore and the solid. Consequently, an increase in pressure will lead to a decrease in the desorption rate.

However, the desorption rate constant (k_d) results in Table 3 increase with pressure. This phenomenon is common in the effect of pressure and temperature on SFE [23]. This phenomenon is commonly referred to as retrograde behavior or crossover phenomenon. At a specific pressure, when the temperature is elevated or reduced, the mole fraction is directly proportional (right graph P_U* and left graph P_L*). However, when the pressure is situated between P_L* and P_U*, the mole

fraction value is inversely proportional to the temperature. This phenomenon is attributed to the distinctive properties of supercritical fluids such as having a density of 0.3 g/mL, a viscosity of 0.1-0.01 cP, and a diffusivity of 0.001-0.0001 cm^2/s.

The findings of this study are in line with the simulation results presented by Campos et al. [24] on the extraction of oleoresin from Marigold/Calendula officinalis and Silva et al. [25] on the extraction of *Baccharis trimera* oil. The k_d value increased as the pressure increased. However, in contrast to the findings of the simulations conducted by Macias-Sanchez et al. [15] on the extraction of carotenoids from *Nannochloropsis gaditana*, the k_d value demonstrated a decrease in the simulations of Macias-Sanchez et al. [15] as the pressure value increased. In addition, simulations conducted by Taher et al. [21] for lipids in *Scenedesmus sp.* also showed a decrease in k value due to the dominant negative effect of diffusivity as opposed to the positive effect of solubility. In the meantime, the results obtained by Kitzberger et al. [26] on the extraction of Shiitake mushroom oil have not yet been published. The results obtained by Getachew et al. [13] showed little effect in increasing the pressure towards the yield. Table 3 below provides a comparison of the k_d parameter values at constant temperature from several researchers.

Table 3. Comparison of D_{AB} values at constant temperature from several studies

P (MPa)	T (K)	k_d (10^{-5}/s)				
		[13]	[23]	[24]	[22]	Current research
12	313	-	-	-	1.66	-
12,5	313	-	-	-	-	5.1
15	313	-	22.89	3.23	2.83	-
20	313	14.2	-	4.86	-	63

In addition to pressure, temperature also exerts an influence on the desorption rate. An increase in temperature will result in the disruption of weak physical bonds. The breaking of these bonds will facilitate the desorption transfer thereby increasing the desorption rate with increasing temperature. This result corroborates the findings of Macias-Sanchez et al. [15] and Taher et al. [20] that indicated that the k_d value tended to increase with increasing temperature as lipids' solubility increased. However, this is contrary to the findings of Kim and Hong [27] indicating that the k_d value tended to decrease when the temperature increased. This was due to higher temperature decreasing the density of the fluid [13]. Table 4 presents a comparison of the k_d parameters at constant pressure.

Table 4. Comparison of k_d values at constant pressure from several studies

P (MPa)	T (K)	k_d (10^{-4}/s)		
		[21]	[13]	Current research
10.34	312	574	-	-
10.34	322	238	-	-
30	313	-	1.42	9
30	323	-	1.65	-
30	333	-	1.95	10

3.3. Effect of pressure and temperature on parameter D_{AB}

At a constant temperature, an increase in pressure will result in an elevation of the density of CO_2. This increase in density will lead to a tightening of the distance between molecules, thereby rendering the solute in the solvent more challenging to move. Consequently, its diffusivity will decline. Therefore, the solute diffusivity value in the solvent will decline as the pressure increases.

As shown in Table 5, the value of solute diffusivity in the solvent (D_{AB}) was observed to increase when the pressure rose. This result is not in accordance with the theory. One of the reasons for this is the retrograde behavior or crossover phenomenon that is common in supercritical fluids for SFE processes. The retrograde phenomenon in SFE has also been identified by several previous studies, including those of Confortin et al. [28] and Mukhopadhyay [23] who provided an explanation for this phenomenon in his book entitled Natural Extract Using Supercritical Carbon Dioxide.

Several studies on D_{AB} parameter estimation have yielded similar results to those observed in this study. Research conducted by Macias-Sanchez et al. [15] and Campos et al. [24] indicated that the D_{AB} value tended to increase as the pressure increased. In contrast, the results of Kitzberger et al. [26] exhibited a slightly different trend with a rise and subsequent decline in the D_{AB} value as the pressure increases. Table 5 presents a comparison of D_{AB} parameter results from various researchers for a constant temperature.

Table 5. Comparison of D_{AB} parameter results from several researchers at constant temperature

P (MPa)	T (K)	D_{AB} (10^{-18} m^2/s)			
		[13]	[22]	[20]	Current research
12	313	-	-	6.12×10^4	-
12,5	313	-	-	-	3.9×10^6
15	313	-	1.18×10^5	1.18×10^5	-
20	313	1.24	3.85×10^5	-	5.83×10^6
30	313	6.44	1.06×10^5	-	3×10^7

Table 6. Comparison of D_{AB} parameter results from several researchers at constant pressure

P (MPa)	T (K)	D_{AB} (10^{-18} m^2/s)		
		[12]	[13]	Current research
30	313	9.97×10^6	6.44	3×10^7
30	323	6.37×10^6	12	-
30	333	3.50×10^6	4.22	5×10^7

The results of this study indicated that the D_{AB} value increases with increasing temperature. This finding is consistent with the research of Macias-Sanchez et al. [15]. As the temperature rises, the density of the solution decreases due to the expansion of the intermolecular distance. This reduction in distance between molecules facilitates the movement of solutes, which in turn enhances the diffusion of solutes in the solvent. Consequently, the D_{AB} value increases with an increase in temperature. The D_{AB} parameter estimation results of this

study are in accordance with the theory and support the results of Macias-Sanchez et al. [15]. Table 6 presents a comparison of D_{AB} parameters at constant pressure.

3.4. Accumulation yield

The values of process parameters obtained from simulations and experiments are crucial for validation and error calculation. Validation involves comparing the accumulated yield curve from the simulation results with the experimental results. If the two curves coincide, the process parameter values are appropriate. To compare with the experimental results, the simulation results curve, represented as an instantaneous concentration curve (mol/m^3), needs to be converted into an accumulation yield curve (g solute/100 g dry biomass). This involves multiplying the instantaneous concentration value by the flow rate, preparing a time range, integrating the curve from t_0 to the first-time span, and converting the accumulated mole value to accumulated yield using Equation (11).

$$yield = \frac{100 C_1 M r_{sol}}{m_b} \quad (11)$$

Table 7 presents the results of converting the simulated instantaneous concentration curve (mol/m^3) into a simulated accumulated yield curve (g/100g biomass).

Table 7. Result of conversion of instantaneous concentration curve into accumulation yield curve

	Time (s)	Experiment Yield (g/100g)	Simulation Yield (g/100g)
SFE1	1714.3	1.2	1.23
	5357.1	3.8	4.12
	10285.7	6.7	7.04
	15535.7	9.0	9.35
	18857.1	10.1	10.63
SFE2	1928.6	2.5	3.39
	5464.3	11.0	13.20
	9428.6	19.0	21.19
	12642.9	23.2	24.86
	18428.6	27.3	27.78
	22500.0	28.7	28.36
SFE3	1821.4	6.8	7.45
	5357.1	21.4	20.17
	9000.0	28.0	27.97
	13242.9	32.4	33.18
	17957.1	33.5	34.55
SFE4	2357.1	9.8	10.20
	4928.6	20.8	19.13
	8571.4	30.0	28.24
	13285.7	33.0	33.57
	18000.0	34.0	35.03
	21857.1	34.5	35.55

Fig. 1 compares the accumulation curve of simulation results with the accumulation curve of experimental results for SFE1 under operating conditions of P = 12.5 MPa and T = 313 K. Similarly, Fig. 2 compares the accumulation curve of simulation results with the accumulation curve of experimental results for SFE2 under operating conditions of P = 20 MPa and T = 313 K. Similarly, Fig. 3 shows a comparison between the accumulation curve of simulation results and the accumulation curve of experimental results for SFE3 under operating conditions of P = 30 MPa and T = 313 K. Similarly, Fig. 4 compares the accumulation curve of simulation results with the accumulation curve of experimental results for SFE4 under operating conditions of P = 30 MPa and T = 333 K.

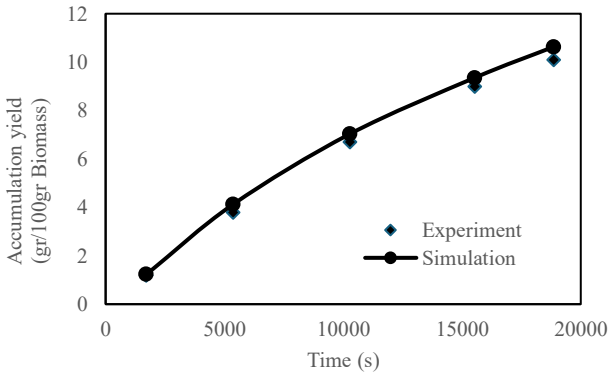

Fig. 1. Comparison Curve of Experimental Accumulation Yield and SFE1 Simulation

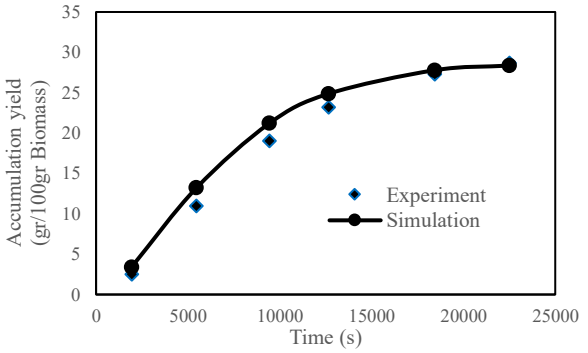

Fig. 2. Comparison Curve of Experimental Accumulation Yield and SFE2 Simulation

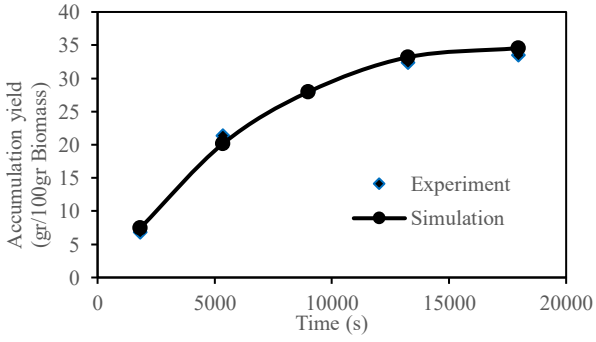

Fig. 3. Comparison Curve of Experimental Accumulation Yield and SFE3 Simulation

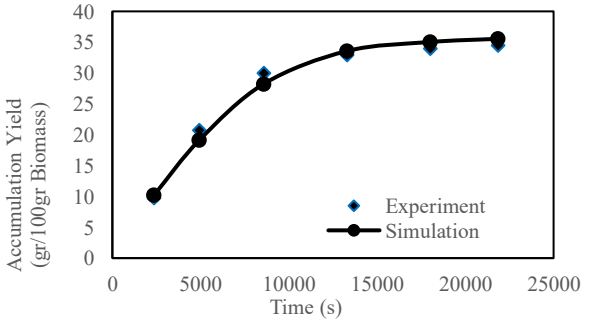

Fig. 4. Comparison Curve of Experimental Accumulation Yield and SFE4 Simulation

4. Conclusion

The desorption rate constant (k_d) obtained at a pressure of 12.5 MPa and a temperature of 313 K was 5.1×10^{-5}/s, at a pressure of 20 MPa and a temperature of 313 K was 6.3×10^{-4}/s, at a pressure of 30 MPa and a temperature of 313 K was 9×10^{-4}/s, and at a pressure of 30 MPa and a temperature of 333 K it is 1×10^{-3}/s. The binary diffusivity (D_{AB}) obtained at a pressure of 12.5 MPa and a temperature of 313 K was 3.9×10^{-12} m^2/s, at a pressure of 20 MPa and a temperature of 313 K was 5.8×10^{-12} m^2/s, at a pressure of 30 MPa and a temperature of 313 K was 3×10^{-11} m^2/s, and at a pressure of 30 MPa and a temperature of 333 K it was 5×10^{-11} m^2/s. k_d and D_{AB} values increase with increasing temperature and pressure. Furthermore, high pressure can result in the mechanical disruption of the solute bond with the solid matrix, which in turn leads to an increase in the k_d. Similarly, high temperature can cause thermal disruption of the solute bond with the solid matrix, resulting in an increase in the k_d.

References

1. S. Singh, D.K. Verma, M. Thakur, S. Tripathy, A.R. Patel, N. Shah, et al., *Supercritical fluid extraction (SCFE) as green extraction technology for high-value metabolites of algae, its potential trends in food and human health*, Food Res. Int. 150 (2021) 110746.
2. G. Dragone, B. Fernandes, A. A. Vicente and J. A. Teixeira, *Third generation biofuels from microalgae in Current Research, Technology and Education Topics*, in: A. Mendez-Vilas (Eds.), *Current Research, Technology and Education Topics in Applied Microbiology and Microbial Biotechnology*. Norristown, PA: Formatex Research Center, 2010.
3. C.J. Diaz, K.J. Douglas, K. Kang, A.L. Kolarik, R. Malinovski, Y. Torres-Tiji, et al., *Developing algae as a sustainable food source*, Front. Nutr. 9 (2022) 1029841.
4. Y. Chisti, *Biodiesel from microalgae*, Biotechnol. Adv. 25 (2007) 294–306.
5. Budiman, *Penentuan intensitas cahaya optimum pada pertumbuhan dan kadar lipid mikroalga Nannochloropsis oculata*, Master Thesis, Institut Teknologi Surabaya, Indonesia, 2010.
6. S.C. Sousa, A.C. Freitas, A.M. Gomes and A.P. Carvalho, *Extraction of Nannochloropsis Fatty Acids Using Different Green Technologies: The Current Path*, Mar. Drugs 21 (2023) 365.
7. E. W. Becker. *Microalgae: Biotechnology and Microbiology*. Cambridge, UK: Cambridge University Press, 1994.
8. B.P. Nobre, F. Villalobos, B.E. Barragán, A.C. Oliveira, A.P. Batista, P.A.S.S. Marques, et al., *A biorefinery from Nannochloropsis sp. microalga – Extraction of oils and pigments. Production of biohydrogen from the leftover biomass*, Bioresour. Technol. 135 (2013) 128-136.
9. A. Mouahid, C. Crampon, S.-A.A. Toudji and E. Badens, *Effects of high water content and drying pre-treatment on supercritical CO_2 extraction from Dunaliella Salina Microalgae: Experiments and modelling*, J. Supercrit. Fluids 116 (2016) 271–280.
10. E. Balboa, A. Moure and H. Domínguez, *Valorization of sargassum muticum biomass according to the biorefinery concept*, Mar. Drugs 13 (2015) 3745–3760.
11. B. Gilbert-López, J.A. Mendiola, L.A.M. van den Broek, B. Houweling-Tan, L. Sijtsma, A. Cifuentes, et al., *Green compressed fluid technologies for downstream processing of Scenedesmus Obliquus in a biorefinery approach*, Algal Res. 24 (2017) 111–121.
12. A. del Sánchez-Camargo, N. Pleite, J.A. Mendiola, A. Cifuentes, M. Herrero, B. Gilbert-López, et al., *Development of green extraction processes for Nannochloropsis gaditana biomass valorization,* Electrophoresis 39 (2018) 1875–1883.
13. A.T. Getachew, C. Jacobsen and A.M. Sørensen, *Supercritical CO2 for efficient extraction of high-quality starfish (Asterias rubens) oil*, J. Supercrit. Fluids 206 (2024) 106161.
14. E. Uquiche, I. Leal and C. Marillán, *Effect of process parameters on the extraction kinetics of Leptocarpha rivularis DC. in a packed bed extractor using supercritical carbon dioxide*, J. Supercrit. Fluids 211 (2024) 106314.
15. M.D. Macías-Sánchez, C.M. Serrano, M.R. Rodríguez and E. Martínez de la Ossa, *Kinetics of the supercritical fluid extraction of carotenoids from microalgae with CO_2 and ethanol as cosolvent*, Chem. Eng. J. 150 (2009) 104–113.
16. R. Arbianti, Angelina, B. Suryapranata, L.P. Latifah, N.F. Putri, T.S. Utami, et al., *Combined enzymatic and ultrasound-assisted aqueous two-phase extraction of antidiabetic flavonoid compounds from Strobilanthes crispus leaves*, Commun. Sci. Technol. 8 (2023) 113-123.
17. S. Tzima, I. Georgiopoulou, V. Louli and K. Magoulas, *Recent Advances in Supercritical CO_2 Extraction of Pigments, Lipids and Bioactive Compounds from Microalgae*, Molecules 28 (2023) 1410.
18. A. Mouahid, K. Seengeon, M. Martino, C. Crampon, A. Kramer and E. Badens, *Selective extraction of neutral lipids and pigments from Nannochloropsis salina and Nannochloropsis maritima using supercritical CO_2 extraction: Effects of process parameters and pre-treatment*, J. Supercrit. Fluids 165 (2020) 104934.
19. Z. Huang, X. Shi and W. Jiang, *Theoretical models for supercritical fluid extraction*, J. Chromatogr. A 1250 (2012) 2–26.
20. H.S. Kusuma, P.D. Amelia, C. Admiralia and M. Mahfud, *Kinetics study of oil extraction from Citrus auranticum L. by solvent-free microwave extraction*, Commun. Sci. Technol. 1 (2016) 15-18.
21. H. Taher, S. Al-Zuhari, A.H. Al-Marzouqi and Y. H, M. Farid, *Mass transfer modeling of Scenedesmus sp. lipids extracted by supercritical CO_2*, Biomass Bioenergy 70 (2014) 530-541.
22. L. Wetterwald, A. Leybros, G. Fleury, F. Delrue, A. Dimitriades-Lemaire, et al., *Supercritical CO2 extraction of neutral lipids from dry and wet Chlorella vulgaris NIES 227 microalgae for biodiesel production*, J. Environ. Chem. Eng. 11 (2023) 110628.
23. M. Mukhopadhyay. *Natural Extracts Using Supercritical Carbon Dioxide*. Boca Raton, FL: CRC Press, 2000.
24. L.M.A.S. Campos, E.M.Z. Michielin, L. Danielski and S.R.S. Ferreira, *Experimental data and modeling the supercritical fluid extraction of Marigold (calendula officinalis) oleoresin*, J. Supercrit. Fluids 34 (2005) 163–170.
25. D.C.M.N. Silva, L.F.V. Bresciani, R.L. Dalagnol, L. Danielski, R.A. Yunes and S.R.S. Ferreira, *Supercritical fluid extraction of Carqueja (Baccharis Trimera) oil: Process parameters and composition profiles*, Food Bioprod. Process. 87 (2009) 317–326.
26. C.S.G. Kitzberger, R.H. Lomonaco, E.M.Z. Michielin, L. Danielski, J. Correia and S.R.S. Ferreira, *Supercritical fluid extraction of shiitake oil: Curve modeling and extract composition*, J. Food Eng. 90 (2009) 35–43.
27. K.H. Kim and J. Hong, *Desorption kinetic model for supercritical fluid extraction of Spearmint Leaf Oil*, Sep. Sci. Technol. 36 (2001) 1437–1450.
28. T.C. Confortin, I. Todero, N.I. Canabarro, L. Luft, G.A. Ugalde, J.R. Neto, et al., *Supercritical CO_2 extraction of compounds from different aerial parts of Senecio brasiliensis: Mathematical modeling and effects of parameters on extract quality*, J. Supercrit. Fluids 153 (2019) 104589.

29. E. Uquiche, B. Sánchez, C. Marillán, R. Quevedo, *Simultaneous extraction of lipids and minor lipids from microalga (Nannochloropsis gaditana) and rapeseed (Brassica napus) using supercritical carbon dioxide*, J. Supercrit. Fluids 190 (2022) 105753.

30. S. Ahmadkelayeh, S. Kaur Cheema, K. Hawboldt, *Supercritical CO_2 extraction of lipids and astaxanthin from Atlantic shrimp by-products with static co-solvents: Process optimization and mathematical modeling studies*, J. CO_2 Util. 58 (2022) 101938.